Available online at www.sciencedirect.com
ScienceDirect
Solar Energy Materials & Solar Cells 91 (2007) 829–842
Solar Energy Materials and Solar Cells
www.elsevier.com/locate/solmat

Luminescent layers for enhanced silicon solar cell performance: Up-conversion

A. Shalav[a,b,*], B.S. Richards[c], M.A. Green[a]

[a]Centre of Excellence for Advanced Silicon Photovoltaics and Photonics, University of New South Wales, Sydney NSW 2052, Australia
[b]Opto-Electronic Materials Section, DelftChemTech, Faculty of Applied Sciences, Delft University of Technology, 2628 BL Delft, The Netherlands
[c]School of Engineering and Physical Sciences, Heriot-Watt University, Edinburgh EH14 4AS, UK

Received 15 December 2006; accepted 4 February 2007

Abstract

An up-converting material can generate one high-energy photon for every two or more incident low-energy photons. This material when placed on the rear side of a traditional bi-facial photovoltaic solar cell has the potential to increase the overall efficiency of the PV device by utilising sub-bandgap photons that would otherwise be transmitted through the device. This paper reviews and examines the application of rare-earth doped inorganic phosphors for achieving external quantum efficiencies for sub-bandgap photons for a bi-facial crystalline silicon photovoltaic device. The mechanisms for up-conversion are discussed and recent experimental results on a bi-facial silicon photovoltaic-upconversion device are analysed.
© 2007 Elsevier B.V. All rights reserved.

Keywords: Luminescence; Up-conversion; Erbium, Rare-earths; Solar cells; Photovoltaics; Silicon

1. Introduction

Due to the discrete band structure of semiconductors, only photons with energies equal to or greater than the bandgap energy E_g will be absorbed and may contribute to an electrical output of a photovoltaic (PV) device. Photons of higher energy, although absorbed, rapidly thermalise to the conduction band edge. The excess photon energy is therefore lost as heat within the lattice of the semiconductor. Photons of lower energy are transmitted through the solar cell and do not contribute to the electrical output. As a result, a compromise between thermalisation and sub-bandgap losses exist when selecting a semiconductor material for PV applications.

Although many semiconductors have a bandgap suitable for the creation of electron-hole (e^--h^+) pairs from solar radiation, silicon (Si) based structures alone have dominated the commercial market. In 2005 alone, 85% of the world's PV production utilised single crystal and multi-crystalline Si [1], and 94% including other Si technologies (for example, a-Si, Si ribbon) [2]. Si has many advantages as a PV material including abundance, non-toxicity and ease of passivation and texturing.

First generation crystalline PV devices although having relatively high efficiencies, also suffer from quite high material costs. Second generation devices, however, although having relatively low costs, unfortunately suffer from quite low efficiencies. A third generation device would be the articulation of these two generations and would benefit by being both highly efficient and inexpensive [3]. It is believed that such a device would be the evolution of second generation thin-film technology with energy conversion efficiencies over the theoretical 31% approaching values closer to the thermodynamic limit of 93% [4]. There are currently five dominant third generation concepts, discussed in detail by Green [4], Martí and Luque [5] and Werner [6] and references within.

The concept of photon conversion is fundamentally different from the other third generation concepts. Photon conversion processes aim at converting via luminescence the solar spectrum to match the absorption properties of

*Corresponding author. Opto-Electronic Materials Section, DelftChemTech, Faculty of Applied Sciences, Delft University of Technology, 2628 BL Delft, The Netherlands.
E-mail address: a.shalav@tudelft.nl (A. Shalav).

0927-0248/$ - see front matter © 2007 Elsevier B.V. All rights reserved.
doi:10.1016/j.solmat.2007.02.007

the semiconductor device. This is in contrast to the other concepts which all focus on developing a semiconductor device better able to match the polychromatic solar spectrum. Consequently, photon conversion processes have a number of advantages over other third generation concepts. Photon conversion can be treated and modelled as an optical process alone, dissociated from the actual operating semiconductor device physics of the solar cell. As a result, photon conversion materials could be applied to existing first and second generation PV single junction devices. Many of these photon conversion processes for PV applications are currently being investigated as part of the FULLSPECTRUM project sponsored by the European Commission under the Sixth Framework Programme [7]. There are three photon conversion processes of interest, namely, down-shifting, down-conversion (DC) and up-conversion (UC). These processes are illustrated schematically in Fig. 1.

Of the three photon conversion processes, both DC and UC are of particular importance since they are both multi-photon processes that are able to minimise thermalisation and sub-bandgap losses, respectively, from a single junction PV device. It has been suggested that an optimised up- and down-converter may be stacked behind and in front (respectively) of an existing bi-facial solar cell and may contribute to an increase in overall efficiency [8–10]. Recently, these processes [11,12] and potential materials [13] for Si-PV applications have been reviewed. An in-depth analysis of rare-earth (RE) doped phosphors for Si-PV down-conversion applications has also been recently presented [14]. A typical photovoltaic-upconversion (PV-UC) device would have three separate layers, ① the bi-facial Si solar cell, ② the phosphors (or other UC material) in a transparent medium and finally, ③ the rear reflector as denoted in Fig. 2.

The impurity photovoltaic effect (IPV) is related to the UC concept except that an IPV device has the 'up-converting' material doped into the bulk of the PV substrate. This dopant gives rise to intermediate impurity energy levels where the up-conversion may occur and has been investigated by Keevers et al. [15,16]. The UC concept examined in this study is optically independent of the bulk of the solar cell, but can be compared with IPV results. Although theoretical optical PV-UC limits have been discussed [9], the practical application and analysis of the UC mechanisms within RE doped materials for PV purposes has not yet been thoroughly investigated for crystalline Si-PV applications.

2. The potential for UC

Using a detailed balance model as proposed by Henry [17], the thermalisation η_{therm}, sub-bandgap η_{sub} and radiative η_{rad} efficiency losses can be graphically interpreted and compared with the maximum energy conversion efficiency η of an ideal solar cell with a given bandgap under air mass 1.5 global (AM1.5G) non-concentrated conditions. Under these conditions: $\eta + \eta_{\text{therm}} + \eta_{\text{sub}} + \eta_{\text{rad}} = 1$, as illustrated in Fig. 3. This model predicts that the maximum limiting energy conversion efficiency $\eta_{\max}$ under AM1.5G(1× concentration) conditions is 31% for an ideal semiconductor with a bandgap of 1.35 eV. These results are very similar to those calculated by Shockley and Queisser under ideal (6000 K) blackbody(1×) conditions, with a maximum η close to 30% for a bandgap of 1.3 eV [18].

UC has the potential to increase the conversion efficiency η by reducing the sub-bandgap component loss η_{sub}. The component η_{sub} is a function dependent on the

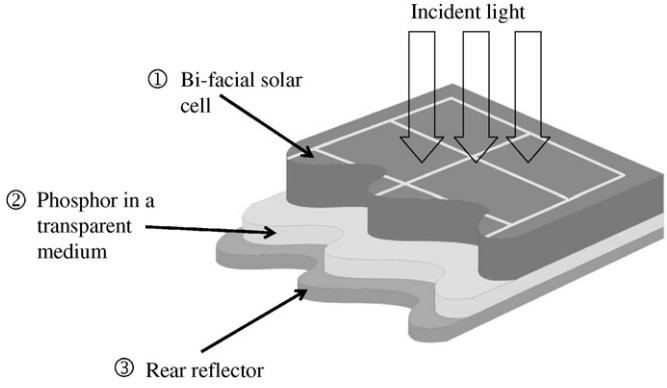

Fig. 2. Cross-section of a three-layered PV-UC device.

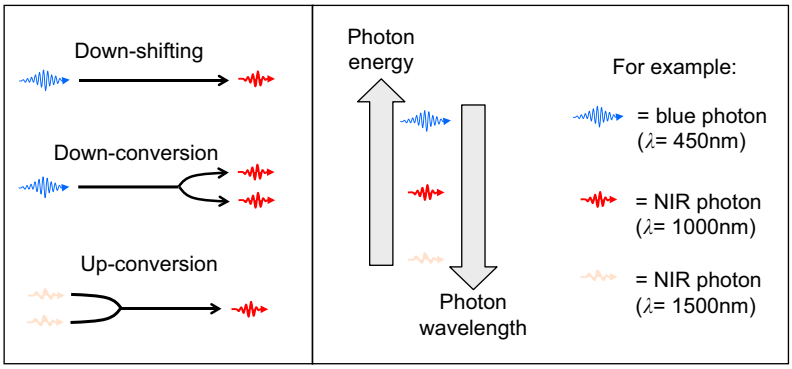

Fig. 1. Photon luminescent conversion processes. Both down- and up-conversion involve multiple photons and are therefore considered 'multi-photon' mechanisms. Only two photon processes are shown for illustrative purposes.

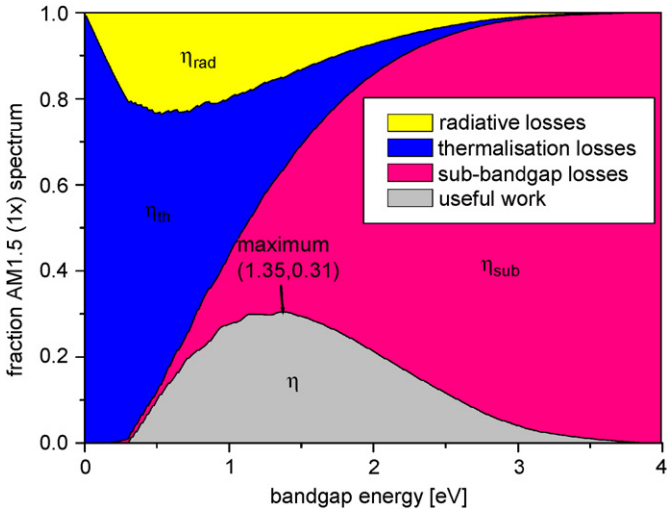

Fig. 3. Theoretical one sun AM1.5G(1×) spectra fractional intensity losses and limiting efficiencies for different ideal bandgap devices (at 300 K). Lower bandgaps have high thermalisation (and radiation losses) whereas higher bandgaps have large sub-bandgap losses.

semiconductor bandgap and the AM of the incident solar radiation. Under AM1.5G(1×) conditions, ideal semiconductors with bandgaps between 0.9 and 1.8 eV, have η values over 25% as calculated using the detailed balance model. These efficiencies are close to the measured efficiency of a passivated emitter rear locally diffused (PERL) cell under similar conditions (24.7%), but for different reasons, all the bandgaps examined have different thermalisation and sub-bandgap losses. Bandgaps below about 1.25 eV have larger thermalisation losses ($\eta_{\text{therm}} > \eta_{\text{sub}}$) whereas bandgaps above 1.25 eV have larger sub-bandgap losses ($\eta_{\text{therm}} < \eta_{\text{sub}}$). It is reasonable to conclude that under such conditions, bandgaps above 1.25 eV would be suited for UC, whereas $E_g < 1.25$ eV would be better suited for down-conversion applications. UC also allows the use of larger band-gap materials to utilise the solar spectrum.

The calculated upper limit of the energy conversion efficiency of a device utilising a two-step UC process has been theoretically investigated by Trupke et al. [9] utilising the theory of detailed balance. The three-level, two-step UC process is modelled using three separate semiconducting diode-type devices, similar to a three cell tandem. The first two diodes act as low bandgap solar cells absorbing near infrared (NIR) photons. These solar cells then drive a highly efficient light emitting diode (LED) that emits photons with a chemical potential equal to the sum of the split in the quasi-fermi energies of the low bandgap solar cells. The solar cells are connected in series to the LED resulting with the added constraint that the currents through each of these devices must be equal. This works best if the LED is highly forward biased. The upper limit of the energy conversion efficiency of the system is calculated to be 63.2% for concentrated sunlight and 47.6% for non-concentrated (blackbody approximated) sunlight. This model, although giving UC limiting efficiencies, is very similar to that for a tandem device utilising a combination of three idealised solar cells.

For a practical UC device, the UC process would occur using a multi-level luminescent material rather than from a multiple solar cell configuration. UC materials currently being investigated for PV applications include both organic (for example porphyrin macrocycles/polyflourenes [19] and TiO_2/dye combinations [20]) and inorganic (for example, quantum dots) materials. Inorganic trivalent rare-earth ions have discrete energy levels with the potential for the UC process to occur from the individual ions alone. The physical processes governing UC and luminescent properties of these ions depend on energy level populations. These populations are highly dependent on rather complicated inorganic atomic principles and are not readily modelled using a combination of idealised semiconducting diode-type devices.

3. REs and up-conversion

REs include both the lanthanides (atomic numbers 57–71) and the actinides (atomic numbers 89–103) and are not so rare as their name implies. Szabadvary [21] has written an in-depth review on the 200+ year history and separation of REs. REs have unique luminescent properties and are considered to be non-toxic [22] making them ideal for a number of modern day commercial applications.

Research and applications using lanthanides have dominated over actinides. One reason for this is that lanthanides have luminescent properties covering the ultraviolet (UV), visible and NIR wavelengths which have been exploited in many applications including lasers, fibre amplifiers and phosphors (as used in fluorescent lighting and cathode-ray tubes). Lanthanides are particularly common in their ionised trivalent state, henceforth denoted as RE^{3+}, and are commonly investigated for their luminescent properties. Literature covering the spectroscopic studies of RE^{3+} ions is mostly technical and aimed predominantly at inorganic chemists who have a detailed understanding of quantum chemistry. The recent developments of RE^{3+} ions to commercial applications has resulted in a number of engineering and introductory texts being written bridging the gap between the inorganic chemistry of RE^{3+} spectroscopy and the larger multi-disciplinary scientific community. Of particular interest for PV-UC applications are texts describing erbium doped fibre optic amplifiers, see for example Refs. [23–25], as well as those describing introductory inorganic optical spectroscopy, for example Ref. [26].

UC utilises the 'ladder' formation of the discrete energy levels from an ion. By absorbing lower energy photons, an electron is able to 'step up' to higher energy levels. If more than two steps are made and the electron then drops back to the ground state ('falls off the ladder'), then a photon is emitted which has a greater energy than any of the initially absorbed photons. All the elements (in their ion forms) of the periodic table with more than one discrete energy level

have the potential to be used for UC applications. There exists a large amount of literature on UC, particularly from lanthanides, actinides and transition metals (see Auzel [27] for an in-depth review). These elements have luminescent energy levels which do not substantially deviate when doped into different materials due to shielded electron levels. This is an important property since it is therefore the host material that will determine the non-radiative rates of the luminescent ion. Most of the research on these materials focus on achieving lasing at specific visible wavelengths via NIR excitation, rather than NIR ($E > 1.1$ eV) emission that would be best-suited for Si solar cells.

Trivalent erbium (Er^{3+}) is an ideal candidate for single wavelength NIR UC for Si-PV applications since it has a ladder of nearly equally spaced energy levels that are multiples of the $^4I_{15/2}-{}^4I_{13/2}$ transition absorbing/emitting photons with energies between 6300 and 6700 cm^{-1} (1480–1580 nm), as shown in Fig. 4. Er^{3+} is also an ideal material to investigate for PV applications since the spectral power from the normalised AM1.5 spectrum yields almost 25 Wm^{-2} in the range 1480–1580 nm. Fig. 4 shows possible 'steps' taken to reach a given Er^{3+} level with energies less than 20 000 cm^{-1}. Intermediate levels that cannot be reached by direct transitions can be bridged using phonons. The phonons available will depend on the host material in which the Er^{3+} ions are doped and the temperature. It can be seen that the $^4S_{3/2}$ level can be reached either by three direct transitions, that is a direct three photon non-simultaneous absorption process, or a four-photon process bridged using two-phonon processes. Defining '$\mapsto$' to represent photon absorption and '$\hookrightarrow$' to represent phonon emission to the lattice, then the three-step direct process follows the route $^4I_{15/2}\mapsto{}^4I_{13/2}\mapsto{}^4I_{9/2}\mapsto{}^4S_{3/2}$, whereas the four-step phonon assisted process follows the route $^4I_{15/2}\mapsto{}^4I_{13/2}\mapsto{}^4I_{9/2}\hookrightarrow{}^4I_{11/2}\mapsto{}^4F_{9/2}\hookrightarrow{}^4I_{9/2}\mapsto{}^4S_{3/2}$.Visible photon emission (about 550 nm) occurs when an electron drops from the $^4S_{3/2}$ to the ground state $^4I_{15/2}$, denoted $^4S_{3/2}\rightarrow{}^4I_{15/2}$. This visible photon emitting level is more commonly reached using a two-step 980 nm excitation source and is a common wavelength used to excite Er^{3+} doped materials for visible UC applications (that is, following the route $^4I_{15/2}\mapsto{}^4I_{11/2}\mapsto{}^4S_{3/2}$, with similar energy level separations).

3.1. Dominant up-conversion mechanisms

There are many mechanisms which can excite an electron to a higher energy level within a trivalent ionised RE resulting in UC luminescence. A few of the dominant mechanisms are summarised below. For illustrative purposes, Er^{3+} ions are used as examples although the mechanisms also apply for other RE^{3+} ions and luminescent centres.

3.1.1. Ground state absorption/excited state absorption (GSA/ESA)

The simplest and most logical UC mechanism involves a ground state absorption (GSA) process followed by an excited state absorption (ESA) process as illustrated in Fig. 4. GSA/ESA UC occurs when photons are absorbed sequentially within a single ion raising its energy to a higher energy state.

3.1.2. Energy transfer up-conversion (ETU)

The energy transfer up-conversion (ETU) mechanism occurs when a nearby excited ion (the 'sensitiser') transfers its energy to a neighbouring ion (the 'activator'), also in an excited state raising it to a higher energy excited state, this is denoted by ①, ② and ③ for a one-, two- and three-step ETU process respectively as illustrated in Fig. 5. For a two-step ETU process, both ions must be in their first excited state before energy can be transferred. This first excited state can be achieved by GSA, or by energy transfer from a neighbouring ion (denoted by ① in Fig. 5). The sensitiser should have a metastable level with a similar energy to that of an excited activator. The energy transfer process

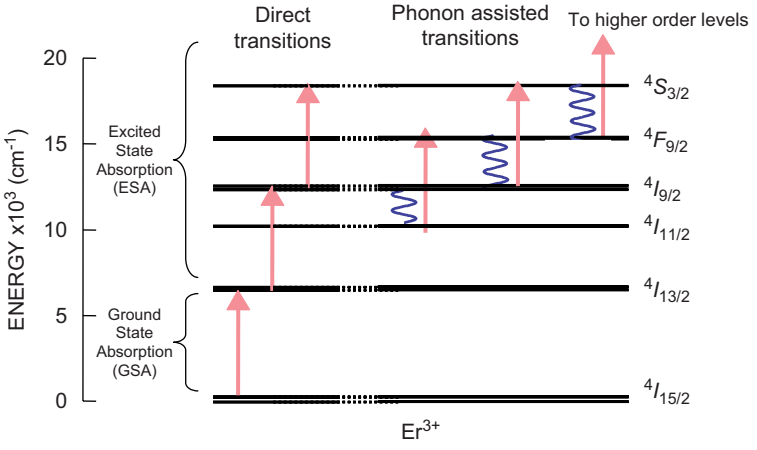

Fig. 4. Energy levels for Er^{3+} showing possible multi-step UC processes. A solid arrow represents a single photon absorption event. This photon has a wavelength between 1480 and 1580 nm. The wavy line represents phonon emission, or energy lost to the host lattice as heat.

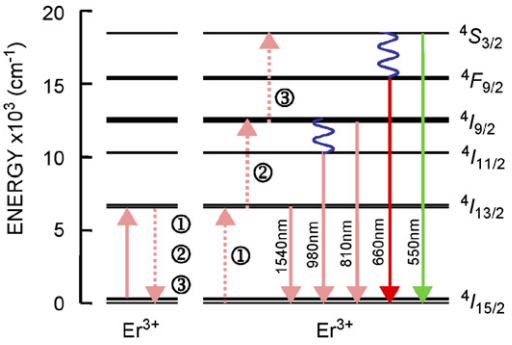

Fig. 5. A three-step ETU process between two Er^{3+} ions. Energy relaxation from one Er^{3+} ion (the sensitiser) can result in energy transfer to a neighbouring Er^{3+} ion (activator) giving rise to higher energy photons. Solid lines represent photon absorption (up) and emission (down), dotted lines represent energy transfer, wavy lines represent phonon emission. For a two-step process, photons with energies greater than the bandgap of silicon are emitted.

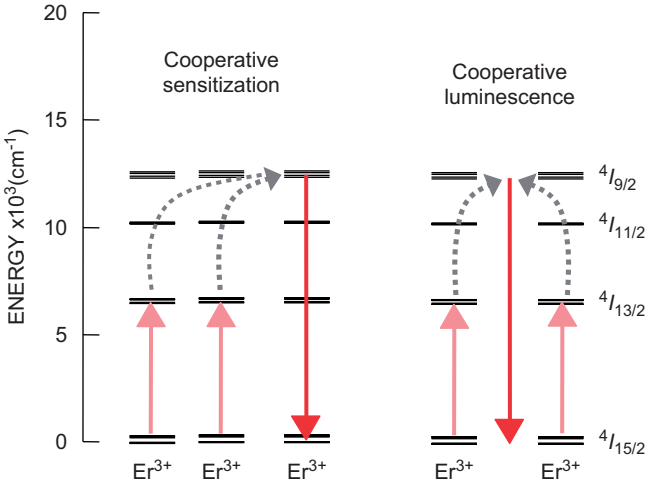

Fig. 6. Co-operative processes between excited neighbouring ions.

denoted by ① could be annotated as $^4I_{13/2} \rightarrow {}^4I_{15/2} \rightleftharpoons I$ $415/2 \rightarrow {}^4I_{13/2}$, where $\rightleftharpoons$ represents the energy transfer mechanism. This energy is transferred by resonant transfer to the activator where the UC luminescence originates. This mechanism is not considered reversible since the probability of finding the system in its initial (excited) state decreases exponentially with time and is consistent with a weak interaction analysis [28].

3.1.3. Co-operative processes

Co-operative UC occurs when two excited neighbouring ions sensitise a third ion (co-operative sensitisation) or combine their luminescent energy (co-operative luminescence), as seen in Fig. 6. The UC luminescence observed from these processes do not necessarily originate from the relaxation of an electron from a higher energy level.

3.1.4. Avalanche up-conversion

Avalanche up-conversion is a result of the efficient population of an excited level due to efficient cross-relaxation processes. Avalanche UC involves a positive feedback system and depends on higher energy level excitations and specific threshold powers to achieve efficient UC. This UC mechanism has been shown to be efficient for visible laser emission using high energy (visible) photons in Er^{3+} doped ZBLAN (a mixture of zirconium, barium, lanthium, aluminum and sodium fluorides) fibres [29] and $LiYF_4$ crystals [30]. This process involving higher excited state energy levels at very high incident threshold pump powers is not practical for solar PV-UC systems and will therefore not be discussed further here.

The UC mechanisms described depend on the lifetime of the intermediate metastable energy levels. The longer an electron is in the excited state, the higher the probability of UC. This is obtained practically by the existence of resonances, for which the ETU mechanism is most suited. For this reason, the ETU mechanism typically has higher UC efficiencies (orders of magnitude) compared with GSA/ESA and co-operative processes [27].

3.2. Dominant up-conversion limiting mechanisms

A number of processes occur which limit the UC luminescent emission. These unwanted effects arise due to the reduction of the excited state population. This process is commonly referred to as 'quenching'. These processes can occur within a single ion or between neighbouring ions and include:

3.2.1. Multi-phonon transitions to lower energy levels

This effect depends on the energy gap between two given levels and the number of phonons required to bridge this gap, and is known as the 'energy gap law', see Section 3.4.2. Typically, if more than six phonons are required to bridge a transition, radiative processes will dominate. To minimise these non-radiative transitions, host materials with low phonon energies should be used.

3.2.2. Radiative emission to lower energy levels

Although radiative emission (for example from an up-converted state to the ground state) is crucial for PV-UC applications, radiative emissions to other sub-levels are also possible. Some of these are lasing transitions and this process is fundamental in the development of NIR lasers around 2800 nm (utilising the $^4I_{11/2}-{}^4I_{13/2}$ transition of Er^{3+}) [31]. A two sub-bandgap photon absorption event (for example GSA/ESA) could also result in the emission of almost two identical photons rather than one which is up-converted following a reverse process of GSA/ESA.

3.2.3. Energy transfer between ions

These (non-upconverting) transfers include energy transfers to other impurity (non-luminescent) ions or energy transfer processes between different luminescent ions, for example cross-relaxation. Fig. 7 shows an example of cross-relaxation occurring. As an example, it is assumed

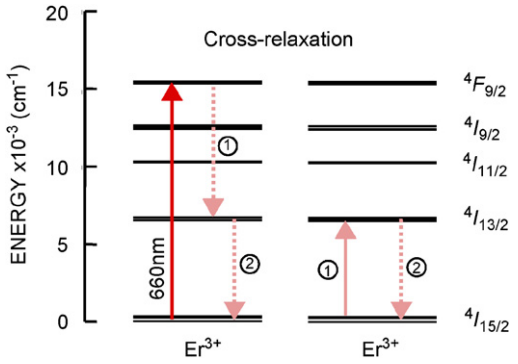

Fig. 7. Cross-relaxation example between two Er^{3+} ions when one ion has been excited to the $^4I_{9/2}$ (980 nm) energy level.

that an electron has been excited (directly or by UC) to the $^4I_{9/2}$ of an Er^{3+} ion (for example, by absorbing a 980 nm photon). The excited electron could then decay from the $^4I_{9/2}$ state to the $^4I_{13/2}$ inducing a second Er^{3+} ion in its ground state to be promoted to $^4I_{13/2}$ (denoted by ① in Fig. 7). This particular cross-relaxation mechanism could be annotated as $^4I_{9/2} \rightarrow {}^4I_{13/2} \rightleftharpoons {}^4I_{15/2} \rightarrow {}^4I_{13/2}$, where $\rightleftharpoons$ represents the cross-relaxation energy transfer process. This could result in the emission of two sub-bandgap photons (denoted by ② in Fig. 7). At high doping levels, efficient non-radiative cross-relaxation processes can dominate due to the increased reabsorption of the UC photons and increased energy coupling between Er^{3+} ions. This effect at high doping levels is called concentration quenching.

3.3. Methods for determining the dominant up-conversion mechanisms

There are a number of experimental techniques which can be performed to determine which UC mechanism dominates a RE^{3+} UC system, particularly for the GSA/ESA and ETU mechanisms.

The fluorescence time profiles for GSA/ESA and ETU mechanisms under pulsed excitations are distinct. Excitation of the energy levels for the GSA/ESA mechanism only occurs during incident light excitation. As a result, the time-dependent fluorescence exponentially decays when the incident illumination is switched off. This differs from the ETU mechanism where UC from energy transfer can occur as long as the intermediate band is still populated [32]. As a result, the time decay profiles can be used to determine if a GSA/ESA or ETU mechanism dominates.

Another method to distinguish the ETU mechanism from that of GSA/ESA is to measure the UC excitation spectrum. Narrowing of the Stark structure of the $^4I_{15/2}$–$^4I_{13/2}$ transition with the process order n is a result of the ETU process [27,33]. This narrowing is illustrated in Fig. 8 for a $n = 1$ to 5 photon process. Co-operative energy transfer effects would show the convolution of all the states involved rather than that of

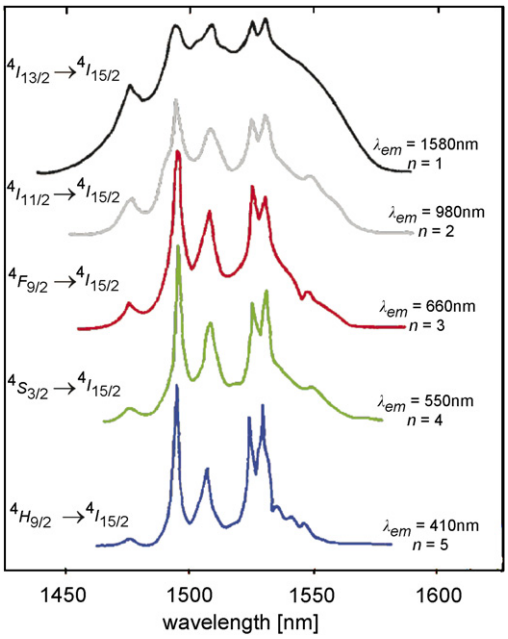

Fig. 8. Excitation spectra (y-axis (a.u)) for n-photon UC from Er^{3+} doped YF_3. Conservation of the Stark structure of the $^4I_{15/2}$–$^4I_{13/2}$ transition implies the ETU mechanism dominates. Adapted from Auzel [27,33].

the excited intermediate $^4I_{15/2}$–$^4I_{13/2}$ transition. Defining the normalised excitation response as $\xi(\lambda, n)$ for an n-step ETU process, then

$$\xi(\lambda, 1) = \xi(\lambda, n)^{1/n}, \tag{1}$$

where $\xi(\lambda, 1)$ represents the initial excitation from $^4I_{15/2} \rightarrow {}^4I_{13/2}$. The shape of the excitation $\xi(\lambda, 1)$ response is often similar to the absorption response between these levels and these responses are often indistinguishable.

3.4. Radiative and non-radiative decay rates

The populations of excited RE^{3+} ions are non-trivial and depend on non-radiative mechanisms such as UC and energy transfer as well as radiative mechanisms to lower energy levels. For a idealised two-level system, the total decay rate A_T from the excited state is given by

$$A_T = A + A^{nr}, \tag{2}$$

where A is the radiative decay rate corresponding to the Einstein coefficient of spontaneous emission, and A^{nr} is the non-radiative decay. The observed lifetime for the resulting fluorescence τ is given by

$$\frac{1}{\tau} = \frac{1}{\tau_0} + A^{nr}, \tag{3}$$

where the radiative lifetime $\tau_0 = 1/A$. Consequently, the radiative quantum efficiency is therefore given by

$$\eta_{rad} = \frac{A}{A + A^{nr}} = \frac{\tau}{\tau_0}. \tag{4}$$

3.4.1. Radiative decay rate calculations

The radiative decay rates for RE^{3+} ions are well known and agree with detailed mathematical models. This section gives a non-mathematical overview into the methods for determining the radiative rates of RE doped materials.

Transitions of 'pure' RE^{3+} ions are parity forbidden transitions. Because of selection rules (for example, the well-known Laporte parity rule from quantum mechanics) dipole transitions can only occur between energy levels with an angular momentum parameter differing by one. This implies that dipole transitions within the 4f level (with the same parity) are dipole-forbidden. However, once these ions are doped into host crystals or glasses, some of these transitions are allowed. The internal electric and magnetic fields of the host can break certain symmetries resulting in a mixing of states with different parity giving rise to weakly allowed transitions. These weakly allowed transitions give rise to the long lifetimes (in the order of μs to ms) of the energy levels of RE^{3+} ions doped into a host material. These 'metastable' levels are crucial for lasing applications and efficient UC processes.

The radiative emission probabilities from electric or magnetic dipole transitions can be calculated using the matrix element of the corresponding interaction Hamiltonian operator taken between the initial and final atomic states [24]. Electric dipole transitions are generally much more intense (around five orders of magnitude) than magnetic dipole allowed transitions [26]. The theoretical calculation for the electric dipole transitions is non-trivial and has many difficulties [34]. The independent theories by Judd [35] and Ofelt [36] in 1962 made it possible to calculate the electric dipole transitions solving many of these difficulties. Judd–Ofelt parameters are constants determined empirically and have been calculated, collected and tabulated for many host materials, see for example Ref. [37]. The oscillator strength for any absorption or emission transition (not necessarily to the ground state) can be easily determined using these parameters for a particular host material. Smakula's formula can be used to experimentally determine the oscillator strength from the absorption spectrum [26]. The density of absorbing centres can also be calculated if the oscillator strength is known. The spontaneous emission probability A can also be written in terms of the oscillator strength f given by García Solé [26].

The probability of radiative emission as compared to non-radiative from $J \rightarrow J'$ levels of a RE^{3+} is strongly related to the energy separation between these levels. The larger the energy gap and the larger the radiative emission rate.

3.4.2. Non-radiative decay rate calculations

Non-radiative processes in a RE^{3+} doped material arise due to phonon emission (and subsequent propagation through the host material). Many experimental investigations performed on low RE^{3+} ion doped host crystals and glasses have shown that the rate of phonon emission decreases exponentially with the corresponding energy gap, see for example Refs. [23,38]. This gives rise to what is commonly referred to as the 'energy gap' law (see for example Ref. [26]) and is expressed as

$$A^{nr} = A^{nr}(0)\exp(-\alpha\Delta E), \tag{5}$$

where $A^{nr}(0)$ and α are constants that depend only on the host material and not on the RE^{3+} ion. ΔE is the energy gap between the two levels. These constants can be found graphically from experimental data. Fig. 9 shows experimental data from different crystal hosts as measured by Weber [38] and plotted on (logarithmic scale) A^{nr} versus (linear) ΔE. The shaded area of Fig. 9 indicates typical radiative rates (10^2–$10^4\ s^{-1}$) as described in Ref. [26]. These constants for glasses used for fibre amplifiers have also been tabulated [25]. Low energy gaps generally result in non-radiative levels (for example, non-radiative rates dominate) compared with larger 'light-emitting' energy gaps. The exponential decrease for larger energy gaps is due to the increase in the number of emitted phonons required to bridge this gap. Phonons that mostly participate in this process are the (highest energy) effective phonons which usually have a large density of states. The number of effective phonons n to bridge an energy gap is calculated by dividing the energy gap by the effective phonon energy.

4. Up-conversion phosphors for Si PV-UC applications

Phosphors have been shown to have high UC efficiencies and can be mixed with a binding/adhesive agent and easily deposited on the rear of a bi-facial cell. There are very few instances in the literature of research being performed on UC phosphors in conjunction with solar cells. In 1983, Saxena [39] described the use of terbium doped lanthanum fluoride and thulium doped calcium tungstate materials for application with PV devices; however, actual measurements with solar cells were never reported.

Non-linear materials have been dominantly used to provide frequency conversion and require high-intensity coherent radiation. UC within RE^{3+} ions only depend on the rate equations of the population levels which are independent on the spatial and temporal coherence of the incident light. As a result, applications utilising low-intensity incoherent NIR light can be realised. Depending on the application, the UC mechanisms are either maximised (for example, solid-state UC lasers [40,41]) or minimised (for example, Er^{3+} doped waveguide amplifiers [42–44]).

Visible luminescent materials using IR wavelengths to excite a RE solid were first proposed in 1959 by Bloembergen [45] and was referred to as 'quantum counter action'. UC research at this time focused on RE^{3+} doped crystals or phosphors. One of the primary applications at the time was to develop an UC laser. With the development of the first solid-state laser, research shifted away from RE^{3+} phosphors and more towards UC RE^{3+} crystals and

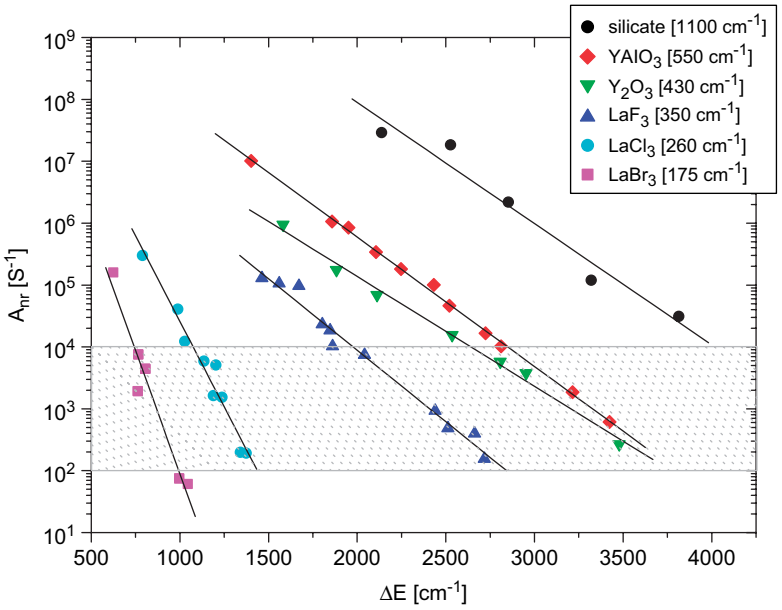

Fig. 9. Non-radiative rates as a function of ΔE. The shaded area represents typical radiative rates. The wavenumber in brackets represents the effective phonon energy of the host (adapted from Weber [38]).

fibres [46]. Primarily UC phosphors were used as coatings for the detection of IR laser beams [47]. Over the years, they have also been used for X-ray storage and IR quantum counting. More recently, UC phosphors have been used in panel colour displays and inks used for secure printing. Many IR detector cards on the market do not use UC phosphors. They do, however, emit higher wavelengths when excited by IR radiation. Such phosphors are known as storage phosphors and have been used for many years, primarily for IR detection [48]. Storage phosphors require pre-charging by exposure to UV or visible light and use a process called electron trapping. Storage phosphors are usually composed of RE doped zinc/cadmium sulfides and selenides [49]. Up until the mid 1990s, most UC phosphors used for IR laser detection had a fluoride host. Intensities two orders of magnitude greater were realised if a chloride (lower phonon energy) host were used [50]. One of the most efficient NIR-visible UC phosphor reported to-date is that of Er^{3+} and trivalent Ytterbium (Yb^{3+}) doped sodium yttrium fluoride ($NaYF_4$). This phosphor utilises the ETU mechanism with Yb^{3+} acting as the sensitiser (around 980–1000 nm) and Er^{3+} as the acceptor resulting in visible luminescence. The $NaYF_4$ was first examined as an efficient UC host in the early 1970s [51,52] but it has only been in the last few years that it has been further investigated for UC applications [53–56], particularly for the application for converting NIR 'waste light' from an incandescent lamp to the visible [54]. More recently, these types of phosphors have been investigated for new emissive display applications [57]. These types of phosphors are not useful for crystalline Si PV-UC applications since the Si andYb^{3+} essentially compete for the NIR photons with wavelengths between 900 and 1100 nm. They may, however, prove useful for higher bandgap materials (for example a-Si or CdTe) where photons with the forementioned wavelength range are now sub-bandgap and the broad, highly absorbing $^2F_{5/2}$ level of the Yb^{3+} ion acts as the intermediate step for UC.

Halide hosted phosphors have smaller phonon energies compared with other hosts [58]. Lower phonon energies are an important attribute for minimising non-radiative (multi-phonon) losses and increases the overall metastable energy lifetime. Phonon energies generally decrease across the halides with increasing atomic number, that is:

larger phonon energy — 600 cm^{-1} — 355 cm^{-1} — 260 cm^{-1} — 172 cm^{-1} — 144 cm^{-1} — smaller phonon energy

$\Leftarrow$ (oxide) > fluoride > chloride > bromide > iodide $\Rightarrow$

(larger excitation spectrum) (smaller excitation spectrum)

where the energies (in cm^{-1}) represent 'typical' highest energy lattice phonons for each halide host as tabulated by Gamelin and Güdel [32]. The relative emitted visible (three-step UC) intensity under 1516 nm (5 mW) excitation for different Er^{3+} doped halides has been measured to be [58]:

fluoride : chloride : bromide : iodide = 1 : 48 : 4 : 0.6,

with the chloride host performing the most favourably. The reason for this is because, although bromide and iodide hosts have low phonon energies, they also have narrower excitation spectrums for the intermediate steps (required for ETU), resulting in less absorption. The larger halides have smaller anionic field strengths (smaller phonons), resulting in smaller Stark splitting and narrower excitation spectra. The increased UC performance of the chlorides implies the ideal host should have not only a low phonon energy, but also a large excitation spectrum. Chloride hosts

are currently being assessed as potential hosts for PV-UC devices [59].

The Raman spectrum of non-doped $NaYF_4$ has been shown to have three fully resolved phonon peaks at 298, 370 and 418 cm^{-1} with a weighted average of close to 360 cm^{-1} [56]. This is considerably lower than other similar structured fluoride host lattices such as lithium yttrium fluoride ($LiYF_4$) which has phonon energies up to 570 cm^{-1} [60]. $LiYF_4$ has been more thoroughly investigated in the literature than $NaYF_4$ and tabulated data tables for $LiYF_4$ are more readily available, see for example Ref. [61]. Structurally, $NaYF_4$ is very similar to $LiYF_4$. The higher coordination number for Y, shorter Y-F distances, weaker bond strengths and the larger mass of Na could be possible reasons why the $NaYF_4$ host has a smaller phonon energies compared to $LiYF_4$ [56]. It has been suggested that the larger phonon energies (the ones of importance for the energy gap law) are from the lithium ions alone in $LiYF_4$ [60] and this has been supported recently by theoretical calculations [62]. It is therefore reasonable to assume that the larger phonon energies from the $NaYF_4$ host are contributed dominantly from the sodium ions. The low phonon energies and relatively broad absorption/excitation spectrum of the $NaYF_4$ crystal make it a very promising host material for RE^{3+} ions for two-step PV-UC applications. An ideal RE^{3+} doped UC material for PV applications needs to be able to attached or adhered to the rear of a bi-facial solar cell. The first paper reporting enhanced PV-UC efficiencies consisted of a 100 μm vitroceramic doped with Er^{3+} and Yb^{3+} on the rear of a substrate-free gallium arsenide (GaAs) solar cell [63]. Unfortunately, the authors concluded that the efficiency of the system was too low for practical application in PVs and no further work was reported.

5. NIR Si-PV enhancement using Erbium doped $NaYF_4$ phosphors

Two prototype devices were fabricated based on the schematic shown in Fig. 2. The first, Device {1}, was made using $NaY_{0.8}F_4 : Er^{3+}_{0.2}$ phosphors and had a rear-diffuse reflector [64,65]. The second, Device {2}, had a specular (evaporated silver) rear. The second device could also be recycled so that the UC effects using different phosphors (for example with different Er^{3+} concentrations) could be compared [66] using the same bi-facial crystalline Si solar cell. Both devices used a crystalline Si double-sided buried contact (DSBC) solar cell. Table 1 summarises the physical layer characteristics of these two devices. A quartz–tungsten–halogen (QTH) lamp was used to measure the external quantum efficiency (EQE) response at lower light intensities, and a Santec TSL-210 tunable laser (1480–1590 nm) was used for intensity-dependent analysis.

5.1. RE^{3+} $NaYF_4$ phosphor synthesis

The synthesis of phase pure $NaYF_4$ is difficult with the final powders consisting of both the efficiently up-converting hexagonal β-phase and poorer up-converting cubic α-phase [56,67]. Recently, the group at the Department of Chemistry and Biochemistry at the University of Bern in Switzerland have optimised a synthesis of high quality μm sized RE^{3+} doped $NaYF_4$ powders in the efficient up-converting β-phase [67]. The phosphors investigated in this study were exclusively made at the University of Bern. The RE^{3+} ions are substituted for the Y in the $NaYF_4$ powder. Other synthesis methods for these types of phosphors have also been recently shown to have good repeatability [68] and controllable aspect ratios [69], attributes important for potential industrialisation.

Initially, 2% and 20% erbium doped sodium yttrium fluoride, $NaY_{0.98}F_4 : Er^{3+}_{0.02}$ and $NaY_{0.8}F_4 : Er^{3+}_{0.2}$, respectively, were synthesised by the group at the University of Bern and investigated as a potential UC phosphors for PV-UC applications. Over the duration of this project, other phosphors were also synthesised and characterised. These phosphors include the additional Er^{3+} doping percentages of 50% and 100%, $NaY_{0.5}F_4 : Er^{3+}_{0.5}$ and $NaErF_4$, respectively, a combination of Er^{3+} and Yb^{3+}, $NaY_{0.6}F_4 : Er^{3+}_{0.2}$, $Yb^{3+}_{0.2}$ along with phosphors doped with Tm^{3+} and Ho^{3+},

Table 1
Device {1} and {2} construction summary

Layer	Parameter	Device {1}	Device {2}
① Cell	Cell type	DSBC	DSBC
	'Upside' down?	No	Yes
	η Facing phosphors	12%	15%
② Phosphor/transparent medium	Er^{3+} Concentration in $NaYF_4$ phosphor	20%	2%, 20%, 50% and 100% 20%Er + 20%Yb
	Medium	*Mattisse* MM4	Solid white oil
	Phosphor:host	3:2	4:1
	Thickness	<0.5 mm	1.6 mm
③ Reflector	Material	White paint	Evaporated Ag
	Type	Diffuse	Specular
	Thickness	0.7 mm	200 nm

If the higher efficiency side of the bi-facial solar cell was placed in contact with the phosphor layer (away from the incident light), the cell is said to be mounted 'upside' down.

$NaY_{0.8}F_4 : Tm^{3+}_{0.2}$ and $NaY_{0.8}F_4 : Ho^{3+}_{0.2}$, respectively. Unfortunately, high-intensity light sources required to excite the lower energy levels of Tm^{3+} and Ho^{3+} phosphors were not readily available and the characterisation of these phosphors was limited. Consequently, this study focusses on the characterisation and application of the Er^{3+} doped samples.

5.2. EQE measurements

The non-linearity of UC light as a function of incident power, P_{in}, affects the predicted EQE of a PV-UC device. For a single energy threshold solar cell, a linear relationship exists between generated e^-–h^+ pairs and number of incident photons, that is, $\phi_{e-h} \propto \phi(\lambda) \propto P_{in}$.

UC processes within RE ions are non-linear and are dependent on radiative and non-radiative transitions, both of which are dependent on the incident light intensity. For this reason, the EQE has a $n-1$ power relationship as given by

$$\mathrm{EQE} \propto \frac{P_{in}^{n}}{P_{in}} \propto P_{in}^{(n-1)}. \quad (6)$$

For an ideal two-step quadratic ($n = 2$) UC process, a linear increase is predicted for the EQE of a PV-UC device for increasing P_{in}. Fig. 10 shows the EQE and calculated internal quantum efficiency (IQE) for the Device 1 configuration. A maximum EQE for the first device had a value close to 5.5×10^{-6} under QTH lamp 1523 nm excitation. This value is only a few times larger than the measurements performed on Er^{3+} doped Si PERL cells (for IPV applications) using a similar excitation source, as published by Dood et al. [70] based on measurements by Keevers et al. [15,16] where an EQE value of close to 2.1×10^{-6} was measured at 1535 nm excitation.

The comparison of EQE measurements for the PV-UC devices and Si doped PERL cells are not meaningful since the solar cell structures differ considerably, the former are planar bi-facial buried contact while the latter are textured

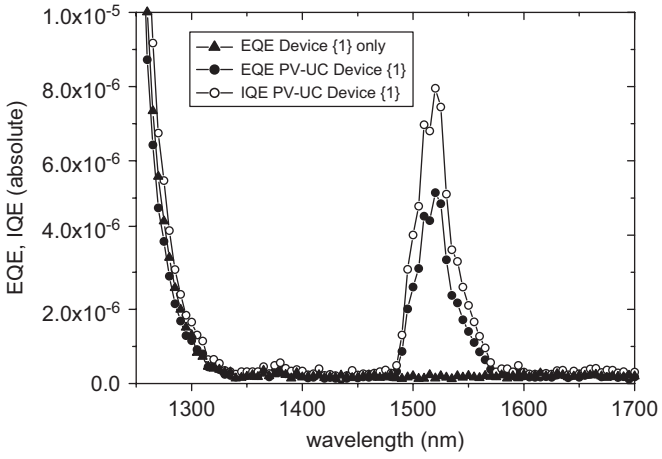

Fig. 10. EQE and calculated IQE spectral response for the PV-UC Device {1}. For comparison purposes, the EQE of the same solar cell is shown without the phosphors attached to the rear (transparent host and white paint only).

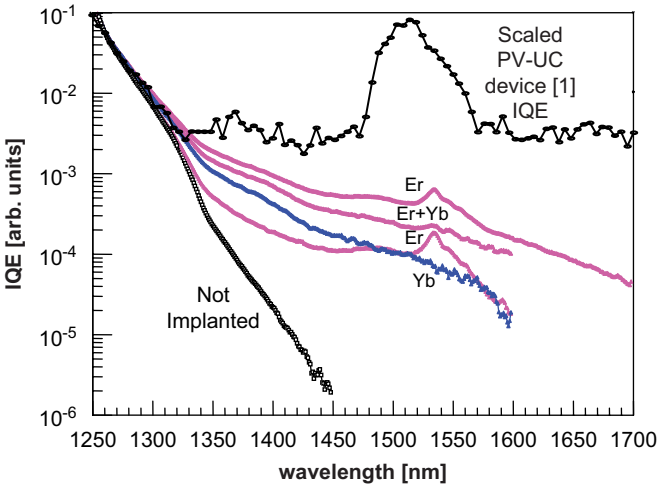

Fig. 11. PV-UC device IQE measurements compared with Er^{3+} doped PERL cells. The IQE from the PV-UC device is more than 2 orders of magnitude larger than compared with Er doped PERL cells (after Keevers et al. [15]). Relative IQE values below about 2×10^{-3} were not observed, most probably due to the sensitivity settings of the experimental setup.

PERL, resulting in different reflection losses at NIR wavelengths. IQE values are therefore more meaningful for comparison purposes at the NIR wavelengths of interest. Furthermore, Keevers has shown that the IQE is proportional to the absorption coefficient at wavelengths sufficiently weak (close to 1200 nm) and where the response is not affected by the Er^{3+} ions [15,16,71]. Therefore, by 'overlaying' (incorporating a shifting of the y-axis) the IQE results for wavelengths close to 1200 nm, it is possible to compare corresponding spectral responses. Fig. 11 shows the IQE calculations from the PV-UC Device {1} overlayed with Er^{3+} doped Si PERL cell responses. Keevers defines the relative IQE as follows: The relative IQE of the implanted cell is normalised to 1 at 1000 nm. The IQEs of all the other cells are normalised to match that of the un-implanted cell at 1180 nm. Likewise, the IQE data from the PV-UC device has been normalised to this value also. Ideally the IQE of the PV-UC device would follow that of the 'not implanted' response for wavelengths less than 1480 nm and greater than 1580 nm. Although the actual measured response within these ranges are consistent with a large background stray light effects [71], the most likely cause is from instrument insensitivity. The IQE measured between 1480 and 1580 nm using the phosphors is more than two orders of magnitude greater than that measured from the Er doped PERL cells suggesting that the UC process from the phosphors is much more efficient than measured from energy coupling between Er and Si IPV approaches.

5.3. EQE power dependence

Fig. 12 shows a log of the short circuit current, $\log(I_{sc})$, versus the log of the incident power, $\log(P_{in})$ using 1523 nm

excitation from a Santec TSL-210 tunable laser for powers up to 5 mW. The slope n is close to 2 for lower powers, but decreases to 1.57 at higher powers. The calculated EQE is close to linear at low powers as predicted by Eq. (6). The EQE begins to depart from the theoretically predicted behaviour at higher powers, as illustrated in Fig. 13. A maximum EQE value of close to 2.5% is measured at these higher values under 1523 nm laser excitation.

The excitation spectrum indicates which wavelengths are capable of exciting a particular luminescent response from a luminescing centre. For a silicon PV-UC device with Er^{3+} doped phosphors, the luminescent response is a result dependent on the number of (up-converted) photons emitted originating from the $^4I_{9/2}$ level of the Er^{3+} ion(s). The normalised excitation response $\xi(\lambda)$ has the same shape as the normalised $I_{sc}(\lambda)$ or EQE(λ) responses at a fixed

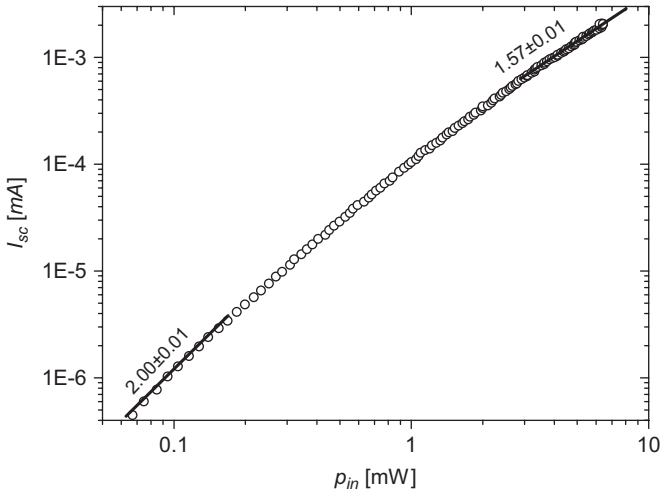

Fig. 12. Log–log plot showing the power law relationship between I_{sc} and P_{in} at high incident powers. These results were measured using a tunable laser source at 1523 nm.

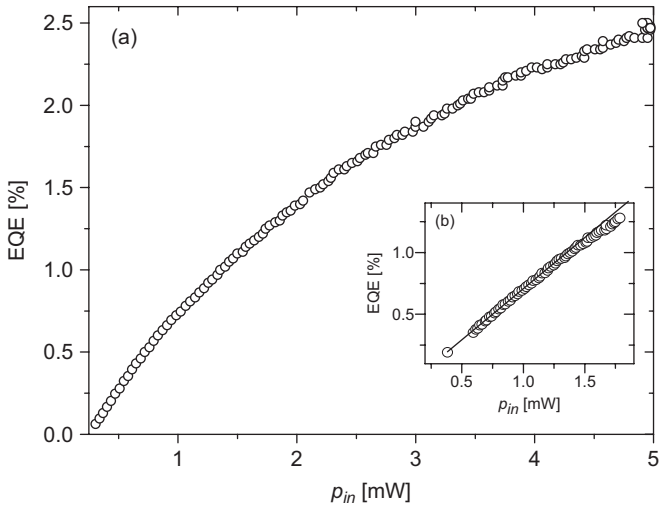

Fig. 13. EQE as a function of P_{in} at 1523 nm. (a) The EQE rises linearly at low powers then begins to level off. (b) High resolution EQE response at low incident powers showing the linear region.

power P_{in}. From Eq. (1), the relationship between two excitation responses, $\xi_1(\lambda, n_1)$ and $\xi_2(\lambda, n_2)$ at different incident powers, P_{1in} at P_{2in}, will be given by

$$\xi_1(\lambda, n_1)^{1/n_1} \approx \xi_2(\lambda, n_2)^{1/n_2}, \tag{7}$$

where n_1 and n_2 is the measured power law dependency at two different bias powers, P_{in1} and P_{in2}. The excitation responses calculated from Eq. (7) will have a similar shape to the absorption of the intermediate $^4I_{15/2}-^4I_{13/2}$ transition. Fig. 14 shows this relationship between the power n law excitation response (from measured I_{sc} or EQE results) and the calculated intermediate level absorption response. Although the absorption and excitation spectra are distinct, they often overlap. Conservation of the excitation (absorption) responses related by Eq. (7) at different incident powers suggests that the dominant mechanism for UC for this device is that of ETU. This relationship is a direct result of the narrowing of the Stark structure of the $^4I_{15/2}-^4I_{13/2}$ transition for a n photon process as illustrated back in Fig. 8. Lower values of n result in broadening of the excitation response. This occurs for low n photon processes and also at high incident powers where a reduction of the idealised integer value(s) of n occur. A study investigating the effect of different doping levels of Er^{3+} within the $NaYF_4$ host using the second device configuration was performed and the effect of different incident intensities investigated [66]. The phosphors investigated included $NaY_{1-x}F_4 : Er^{3+}_x$ where $x = 0.02$, 0.2, 0.5, and 1. The maximum EQE measured was 3.4% at 6 mW 1523 nm excitation using the second prototype device with the 20% Er^{3+} doped phosphors ($NaY_{0.8}F_4 : Er^{3+}_{0.2}$), refer to Fig. 15. This value is close to the optimal 25–30% Er^{3+} concentration in a chloride host

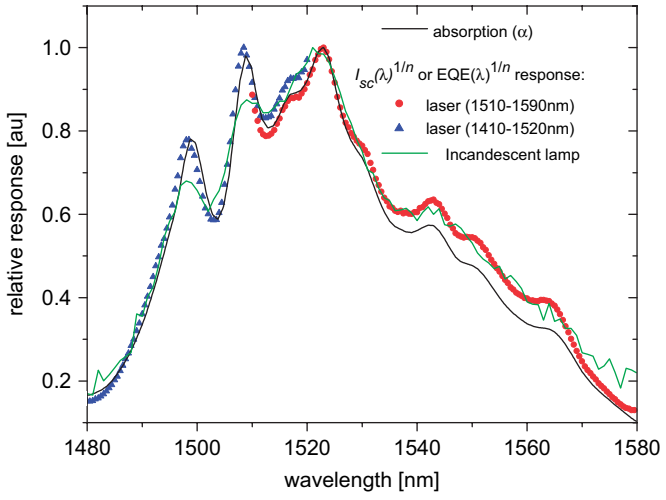

Fig. 14. Excitation/absorption responses. The excitation responses were calculated from normalised I_{sc} values to the power of $1/n$. Under 3 mW excitation, $n \approx 1.57$ was used. For the QTH source, a value for $n \approx 2$ was used. The laser powers were kept at a constant 3 mW for all wavelengths using automatic power control. The absorption spectrum is that calculated using PL emission results.

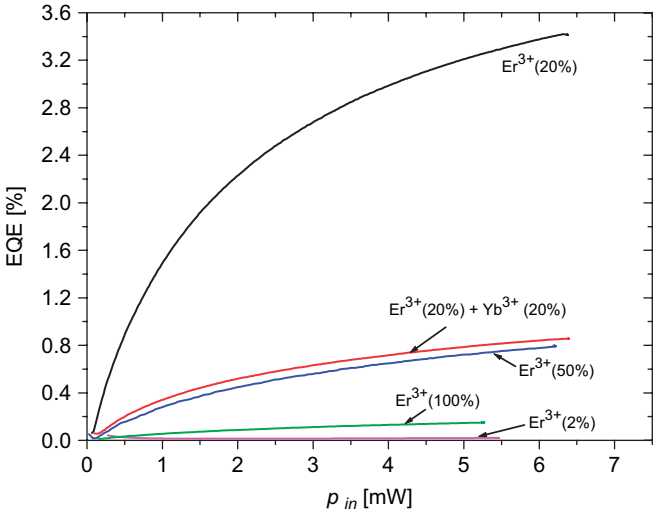

Fig. 15. EQE of PV-UC Device {2} under different P_{in} laser excitation at 1523 nm. The EQE response depends heavily on the doping of the different $NaYF_4$ phosphors. The doping levels are shown on the figure.

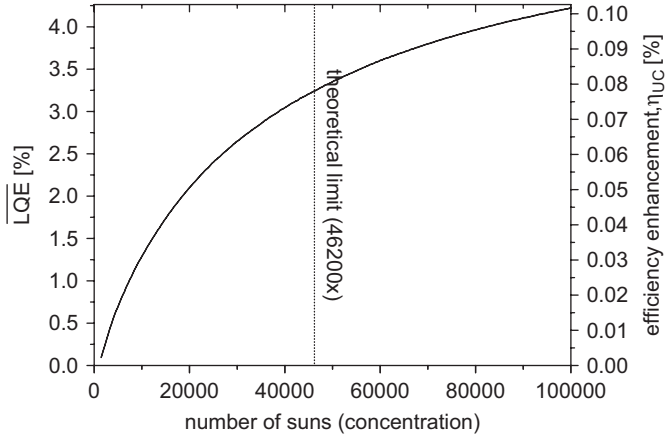

Fig. 16. $\overline{LQE}$ and NIR PV-UC efficiency enhancement, η_{UC}, versus AM1.5G solar concentration. The solar concentration was calculated using the broad absorption properties of the phosphors (1480–1580 nm).

under 1500 nm excitation as measured by Ohwaki and Wang [72].

5.4. Optical losses and the luminescent quantum efficiency

Whereas the EQE is reduced by optical losses within a UC-PV device, the luminescence quantum efficiency (LQE) considers that a photon has already been absorbed within the RE luminescence centre, and can also be regarded as a measure of the UC quantum efficiency. The LQE of the UC-PV device carries a similar definition to the IQE used for solar cells. The LQE was calculated by taking into account the optical losses at the interfaces and in the layers of the PV-UC device, and is determined by

$$\mathrm{LQE} = \frac{\mathrm{EQE}}{(1-L)}, \tag{8}$$

where L represents the losses in the UC-PV device, such as reflection, absorption and non-radiative recombination. The LQE for Device {2} using the $NaY_{0.8}F_4 : Er^{3+}_{0.2}$ phosphors is calculated to be 12.1% at 6 mW, 1523 nm laser excitation.

A practical PV-UC device would be illuminated by the solar spectrum and not a concentrated laser source. It is therefore important to estimate the equivalent number of suns required to obtain a response similar to those measured throughout this project using laser excitation.

The LQE calculated occurs at 1523 nm, a wavelength of maximum absorption. Using EQE measurements, the average response between 1480 and 1580 nm is about a third the maximum response at 1523 nm. This average response between these wavelengths for the LQE will be denoted $\overline{LQE}$. The best case scenario for a PV-UC device is to assume there are minimal losses. In this case, the measured EQE will be approximately equal to the LQE (at sub-bandgap wavelengths). Using these idealised values for the EQE, it is possible to calculate the NIR efficiency enhancement η_{UC} of the PV-UC device at NIR wavelengths under AM1.5G conditions. The total efficiency for such a device will be the energy conversion efficiency of the solar cell, η, plus that of the UC enhancement η_{UC}. Fig. 16 shows the calculated η_{UC} values using $\overline{LQE}$ values for various solar AM1.5G concentrations using the broad absorption properties of the phosphors, that is between 1480 and 1580 nm rather than just the maximum excitation value at 1523 nm. The theoretical concentration limit is also shown in Fig. 16.

6. Conclusions

The $NaYF_4$ host is ideal for up-conversion applications with relatively low energy phonons present. When only doped with Er^{3+} ions, a relatively broad absorption band exists for the intermediate up-conversion transition. This absorption is still relatively narrow when compared to the solar spectrum.

At low incident sub-bandgap power intensities, the ETU mechanism dominates since a quadratic dependence on P_{in} is observed. At higher intensities, higher order up-conversion processes including cross-relaxation, de-populate the intermediate energy level lowering the luminescence from the $^4I_{11/2}$ level and therefore the EQE response of the PV-UC device.

The idealised (LQE $\approx$ EQE) calculated efficiency enhancement using the phosphors investigated in this project are too small and require solar concentrations un-realistic for practical terrestrial crystalline Si PV-UC devices. One of the primary reasons for this low efficiency enhancement is because only a narrow range of wavelengths are utilised (1480–1580 nm). Even if the PV-UC device had a LQE of 100% for this wavelength range, the value of η_{UC} would only be 2.4%.

The phosphors investigated in this study have high luminescent efficiencies once up-conversion occurs, but

suffer from poor infrared absorption and low up-conversion efficiencies. This study suggests that a relatively high doping level of selected RE^{3+} ions into low phonon energy crystals can improve the absorption and luminescent properties of the phosphor. A larger doping level is also required for the efficient ETU mechanism, although higher levels also suffer from losses from higher UC and cross-relaxation mechanisms.

Acknowledgements

The authors would like to thank H.U. Güdel, K.W. Krämer and D. Biner (Department of Chemistry, University of Bern, Switzerland) for supplying the erbium doped $NaYF_4$ phosphors. Also, Peter Cousins and Malcolm Abbott (Centre of Excellence for Advanced Silicon Photovoltaics and Photonics, University of New South Wales, Sydney, Australia) for the Si bi-facial solar cells utilised in this study.

References

[1] P. Maycock, T. Bradford, Renew. Energy World 9 (4) (2006).
[2] T. Bradford, H. Flynn, Renew. Energy World 9 (5) (2006).
[3] M.A. Green, Progr. Photovolt. 9 (2001) 123.
[4] M.A. Green, Third Generation Photovoltaics: Advanced Solar Energy Conversion, Springer, Berlin, Heidelberg, Germany, 2003.
[5] A. Martí, A. Luque (Eds.), Next Generation Photovoltaics: High Efficiency Through Full Spectrum Utilization, Institute of Physics Publishing, Bristol, UK and Philadelphia, PA, 2004.
[6] J. Werner, Adv. Solid State Phys. 44 (2004) 51.
[7] A. Luque, A. Martí, A. Bett, V.M. Andreev, C. Jaussaud, J.A.M. Van Roosmalen, J. Alonso, Sol. Energy Mater. Sol. Cells 87 (2005) 467.
[8] T. Trupke, M.A. Green, P. Würfel, J. Appl. Phys. 92 (3) (2002) 1668.
[9] T. Trupke, M.A. Green, P. Würfel, J. Appl. Phys. 92 (7) (2002) 4117.
[10] T. Trupke, A. Shalav, P. Würfel, M.A. Green, Sol. Energy Mater. Sol. Cells 90 (2006) 3327.
[11] B.S. Richards, Sol. Energy Mater. Sol. Cells 90 (2006) 2329.
[12] B.S. Richards, K.R. McIntosh, Overcoming the poor short wavelength spectral response of CdS/CdTe photovoltaic modules via luminescence down-shifting: ray-tracing simulations, Progr. Photovolt. 15 (1) (2007) 27.
[13] C. Strümpel, M. McCann, G. Beaucarne, V. Arkhipov, A. Slaoui, V. Švrček, C. del Cañizo, I. Tobias, Sol. Energy Mater. Sol. Cells 91 (4) (2006) 238.
[14] B.S. Richards, Sol. Energy Mater. Sol. Cells 90 (2006) 1189.
[15] M. Keevers, F. Saris, G. Zhang, J. Zhao, M.A. Green, Screening of optical dopants in silicon solar cells for improved infrared response, in: 29th IEEE Photovoltaics Specialists Conference Proceedings, 1997, pp. 215–218.
[16] M.J. Keevers, M.A. Green, Sol. Energy Mater. Sol. Cells 41–42 (1996) 195.
[17] C.H. Henry, J. Appl. Phys. 51 (8) (1980) 4494.
[18] W. Shockley, H.J. Queisser, J. Appl. Phys. 32 (3) (1961) 510.
[19] S. Baluschev, T. Miteva, V. Yakutkin, G. Nelles, A. Yasuda, G. Wegner, Phys. Rev. Lett. (2006) 143903.
[20] J.A.M. Van Roosmalen, Semiconductors 38 (8) (2004) 970.
[21] F. Szabadvary, The history of the discovery and separation of the rare earths, in: K. Gschneidner, L. Eyring (Eds.), Handbook on the Physics and Chemistry of Rare Earths, vol. 11, Elsevier Science Publishers, Amsterdam, 1988, pp. 33–80 (Chapter 73).
[22] T. Haley, Toxicity, in: K. Gschneider, L. Eyring (Eds.), Handbook on the Physics and Chemistry of Rare Earth, vol. 4, North-Holland, Amsterdam, 1979, pp. 553–586 (Chapter 40).
[23] P.C. Becker, N.A. Olsson, J.R. Simpson, Erbium-Doped Fiber Amplifiers: Fundamentals and Technology, Academic Press, San Diego, USA, 1999.
[24] E. Desurvire, Erbium Doped Fiber Amplifiers: Principles and Applications, Wiley, USA and Canada, 1994.
[25] M.J.F. Digonnet, Rare-Earth-Doped Fiber Lasers and Amplifiers, Marcel Dekker, NY, USA, 2001.
[26] J. García Solé, L.E. Bausá, D. Jaque, An Introduction to the Optical Spectroscopy of Inorganic Solids, Wiley, England, 2005.
[27] F. Auzel, Chem. Rev. 104 (2004) 139.
[28] T.F. Soules, C.B. Duke, Phys. Rev. B 3 (2) (1971) 262.
[29] F. Auzel, Y. Chen, J. Non-Cryst. Solids 184 (1995) 57.
[30] F. Auzel, Y. Chen, J. Lumin. 65 (1995) 45.
[31] C. Labbé, J.L. Doualan, S. Girard, R. Moncorgé, M. Thuau, J. Phys.: Condens. Matter 12 (2000) 6943.
[32] D. Gamelin, H.U. Güdel, Top. Curr. Chem. 214 (2001) 1.
[33] F. Auzel, J. Lumin. 31–32 (part 2) (1984) 759.
[34] L.A. Riseberg, M.J. Weber, Relaxation phenomena in rare-earth luminescence, in: E. Wolf (Ed.), Progress in Optics, vol. XIV, North-Holland, Amsterdam, 1976.
[35] B.R. Judd, Phys. Rev. 127 (3) (1962) 750.
[36] G.S. Ofelt, J. Chem. Phys. 37 (3) (1962) 511.
[37] C. Görller-Walrand, K. Binnemans, Spectral intensities of f–f transitions, in: K.A. Gschneider, L. Eyring (Eds.), Handbook on the Physics and Chemistry of Rare Earths, vol. 25, Elsevier Science B.V., Amsterdam, 1998, pp. 101–264 (Chapter 167).
[38] M.J. Weber, Rare earth lasers, in: K.A. Gschneidner, L. Eyring (Eds.), Handbook on the Physics and Chemistry of Rare Earths, vol. 4, North-Holland, Amsterdam, 1979, pp. 275–315 (Chapter 35).
[39] V.N. Saxena, Indian J. Pure Appl. Phys. 21 (1983) 306.
[40] T. Gosnell, Selected Papers on Upconversion Lasers, SPIE milestone series, SPIE Optical Engineering Press, 2000.
[41] R.M. MacFarlane, J. Phys. IV C4 (4) (1994) 289.
[42] P. Kik, Energy transfer in erbium doped optical waveguides based on silicon, Ph.D. Thesis, FOM-Institute for Atomic and Molecular Physics, Amsterdam, 2000.
[43] N. Hamelin, P.G. Kik, J.F. Suyver, K. Kikoin, A. Polman, J. Appl. Phys. 88 (9) (2000) 5381.
[44] F. Lucarz, Silicon nanocrystals in erbium-doped silica for optical amplifiers, M.Sc. Thesis, University College London, Department of Electronic and Electrical Engineering Torrington Place, London, United Kingdom, 2003.
[45] N. Bloembergen, Phys. Rev. Lett. 2 (3) (1959) 84.
[46] K. Buschow, R. Cahn, M. Flemings, B. Lischner, E. Kramer, S. Mahajan (Eds.), Encyclopedia of Materials: Science and Technology, vol. 10, Oxford Press, Oxford, 2001, pp. 9456–9458.
[47] Y. Mita, Appl. Phys. Lett. 39 (8) (1981) 587.
[48] F. Urbach, D. Pearlman, H. Hemmendinger, J. Opt. Soc. Am. 36 (7) (1946) 372.
[49] S. Keller, J. Mapes, G. Cheroff, Phys. Rev. 108 (3) (1957) 663.
[50] Y. Wang, J. Ohwaki, J. Appl. Phys. 74 (2) (1993) 1272.
[51] N. Menyuk, K. Dwight, J.W. Pierce, Appl. Phys. Lett. (4) (1972) 159–161.
[52] T. Kano, H. Yamamoto, Y. Otomo, J. Electrochem. Soc. 26 (1) (1972) 137.
[53] J.F. Suyver, J. Grimm, K.W. Krämer, H.U. Güdel, J. Lumin. 114 (2005) 53.
[54] J.F. Suyver, A. Aebischer, D. Biner, P. Gerner, J. Grimm, S. Heer, K.W. Krämer, C. Reinhard, H.U. Güdel, Opt. Mater. 27 (2005) 1111.
[55] J.F. Suyver, A. Aebischer, P. Gerner, S. Garcia-Revilla, H.U. Güdel, Phys. Rev. B 71 (2005) 125123 (1–9).
[56] J.F. Suyver, J. Grimm, M.K. Van Veen, D. Biner, K.W. Krämer, H.U. Güdel, J. Lumin. 117 (2006) 1.
[57] A. Rapaport, J. Milliez, M. Bass, A. Cassanho, H. Jenssen, J. Disp. Tech. 2 (1) (2006) 68.
[58] J. Ohwaki, Y. Wang, Jpn. J. Appl. Phys. 33 (3A) (1994) L334.

[59] C. Strümpel, M. McCann, C. del Cañizo, I. Tobias, P. Fath, Erbium-doped up-converters on silicon solar cells: assessment of the potential, in: 20th European Solar Energy Conference and Exhibition, 2005, pp. 43–46.
[60] S.A. Miller, H.E. Rast, H.H. Caspers, J. Chem. Phys. 52 (8) (1970) 4172.
[61] C.A. Morrison, R.P. Leavitt, Spectroscopic properties of triply ionized lathanides in transparent host crystals, in: K.A. Gschneider, L. Eyring (Eds.), Handbook on the Physics and Chemistry of Rare Earths, North-Holland, Amsterdam, 1982, pp. 461–692.
[62] B. Minisini, Q.A. Wang, F. Tsobnang, J. Phys.: Condens. Matter 17 (2005) 4953.
[63] P. Gibart, F. Auzel, J. Guillaume, K. Zahraman, Jpn. J. Appl. Phys. 35 (8) (1996) 4401.
[64] A. Shalav, B.S. Richards, T. Trupke, R. Corkish, K.W. Krämer, H.U. Güdel, M.A. Green, The application of up-converting phosphors for increased solar cell efficiencies, in: 3rd World Conference on Photovoltaic Energy Conversion, 2003.
[65] A. Shalav, B.S. Richards, T. Trupke, K.W. Krämer, H.U. Güdel, Appl. Phys. Lett. 86 (2005) 013505.
[66] A. Shalav, B.S. Richards, K.W. Krämer, H.U. Güdel, in: 31st IEEE Photovoltaic Specialists Conference, 2005.
[67] K.W. Krämer, D. Biner, G. Frei, H.U. Güdel, M.P. Hehlen, S.R. Lüthi, Chem. Mater. 16 (7) (2004) 1244.
[68] M. Huang, F. Meng, Lumin. 20 (2005) 276.
[69] L. Wang, L. Yadong, Nano Lett. 6 (8) (2006) 1645.
[70] M.J.A. de Dood, P.G. Kik, J.H. Shin, A. Polman, Incorporation, excitation and de-excitation of erbium in crystal silicon, in: Materials Research Society Symposium Proceedings, vol. 422, Materials Research Society, 1996, pp. 219–225.
[71] M.J. Keevers, Improved performance of silicon solar cells by the impurity photovoltaic effect, Ph.D. Thesis, Photovoltaics Special Research Centre, School of Electrical Engineering, The University of New South Wales, Sydney, Australia, 1996.
[72] J. Ohwaki, Y. Wang, Electron. Lett. 29 (4) (1993) 351.